

Hydrogenation of dimethyl 2,5-furandicarboxylate to dimethyl tetrahydrofuran-2,5-dicarboxylate over Ru/HY

Chengfeng Li, Qishen Lyu[†], Zheng Li, Shuliang Yang, Yong Sun, Xing Tang[†], Xianhai Zeng, and Lu Lin

Xiamen Key Laboratory of Clean and High-valued Utilization for Biomass, Fujian Engineering and Research Center of Clean and High-valued Technologies for Biomass, College of Energy, Xiamen University, Xiamen, 361102, P. R. China
(Received 6 January 2023 • Revised 7 March 2023 • Accepted 31 March 2023)

Abstract—The hydrogenation of biomass-based furan compounds is an important step for the catalytic valorization of biobased chemicals. In this work, Ru-based catalysts supported on different supports, such as HY, MgO and Amberlyst-15, were prepared and estimated for the hydrogenation of dimethyl 2,5-furandicarboxylate (FDMC). Among them, Ru/HY provided a desirable yield of 99.4% for tetrahydrofuran-2,5-dicarboxylic acid dimethyl ester (THFDMC) under 90 °C and 3 MPa H₂. Based on catalyst characterization, Ru/HY could offer more surface Ru⁰ species and carbon radical intermediates than other catalysts, which could largely favor the activation of hydrogen and then promote the hydrogenation of FDMC over Ru/HY.

Keywords: Dimethyl Furandicarboxylate, Dimethyl Tetrahydrofurandicarboxylate, Support Effect, Hydrogenation, Carbon Radical Intermediate

INTRODUCTION

As a renewable carbon resource, biomass can be converted into high value-added fuels and chemicals [1-4]. The production and utilization of biomass chemicals can mitigate a series of environmental pollution problems caused by petroleum-based chemicals [5-7]. For example, terephthalic acid (TPA) is the monomer for synthesizing polyethylene terephthalate (PET) that has a huge volume of market with massive carbon emissions [8]. In this context, furandicarboxylic acid (FDCA) and dimethyl furandicarboxylate (FDMC) derived from biomass can be used as monomers for production of furan-based polyesters, which are deemed as promising alternatives for PET with better properties, such as biodegradability, gas barrier property, and high glass transition temperature [9-12]. Compared with FDCA, FDMC has a relatively low boiling point and low polarity, and can sublime at relatively low temperatures, making its separation/purification easier than that of FDCA [13]. In addition, FDMC possesses better thermostability than FDCA, which is beneficial to the synthesis of PEF at high temperature [14].

The oxidative esterification of 5-hydroxymethylfurfural (HMF) to furan-2,5-dimethylcarboxylate (FDMC), a renewable alternative to petroleum-derived polyester materials, possesses high oxidation properties for the synthesis of green furan-based polyester materials. Researchers have devoted much effort to the formation of side chain groups (carboxyl groups) by high oxidation of HMF [15-18], so it is important to retain the side chain carboxyl groups. In addition, selective hydrogenation of furan-based carboxylic acids with retention of the carboxyl group is carried out in two main scenarios: hydrogenation to open the furan ring and complete hydroge-

nation of the furan ring [19]. It has been reported that the hydrogenated furan ring opening product is mainly adipic acid, which is important in chemical production, organic synthesis industry, pharmaceuticals, and lubricant manufacturing. In contrast, complete hydrogenation of the furan ring yields dimethyl tetrahydrofuran-2,5-dicarboxylate (THFDMC), which can also be used as a monomer for the synthesis of polyesters [20].

The catalytic hydrogenation of biomass-derived furans is of crucial importance to the production of value-added chemicals from biomass. Especially, many research works have been devoted to the hydrogenation of HMF and its derivatives [21]. For instance, Kataoka et al. [22] reported that Pt/CeO₂ could offer a 2,5-bis(hydroxymethyl)tetrahydrofuran (BHMTHF) yields of 63% (135 °C, 3 MPa H₂, 24 h). Bottari et al. [23] reported that complete hydrogenation of HMF to BHMTHF was achieved over Pd/Al₂O₃, and gave a desirable BHMTHF yield up to 98% (170 °C, 7 MPa H₂, 1 h). A similar BHMTHF yield of 97.3% was obtained over Ru/MnCo₂O₄ (100 °C, 8.6 MPa H₂, 16 h) [24]. Recently, Perret et al. [25] reported that BHMTHF yield of 99% was also obtained from HMF catalyzed by Ni/Al₂O₃ at 80 °C within 12 h under 2 MPa H₂. In the work reported so far, monometallic catalysts containing elements such as Ru, Pd, Pt, Ni have been usually highly reactive [21]. However, the high cost of precious metals and the easy leaching of nickel species under harsh reaction conditions are problematic. Therefore, we need to stabilize the catalyst by reducing the noble metal loading or by a proper selection of the support preparation.

From what we know, the impact of supports has rarely been discussed by previous authors. Herein, we will discuss the effect of the support on the catalyst and even the hydrogenation reaction. Ru/HY was prepared by impregnation method, and displayed outstanding catalytic performance for the selective hydrogenation of furan ring in FDMC to produce THFDMC. THFDMC yield up to 99.4% was achieved over Ru/HY under relatively moderate conditions

[†]To whom correspondence should be addressed.

E-mail: x.tang@xmu.edu.cn

Copyright by The Korean Institute of Chemical Engineers.

(90 °C, 3 MPa H₂, 4 h). Because of the high reactivity of Ru, the catalyst Ru/HY has both hydrogenation active sites and a large number of Brønsted acid sites. In addition, this catalyst can be applied to the hydrogenation of other furan ring compounds and aromatic compounds with satisfactory yields and selectivity. This work provides some insights for the design of catalysts for the complete hydrogenation of biomass-based furan ring compounds.

EXPERIMENTAL

1. Materials

Dimethyl furandicarboxylate (purity > 98%) was purchased from Shanghai Bide Pharmaceutical Technology Co. Ruthenium trichloride trihydrate (RuCl₃·3H₂O) was purchased from Tianjin Hience Optimum Technology Co. Chloroplatinic acid hexahydrate was purchased from Zhengzhou Ruke Biotechnology Co., zeolite Y, hydrogen and Palladium chloride were purchased from Alfa Aesar, polyvinyl alcohol (PVA) and activated carbon was purchased from Shanghai Maclean Biochemical Technology Co. 5-Hydroxymethylfurfural and diammonium hydrogen phosphate were purchased from Anhui Zesheng Technology Co. Furfural, Amberlyst-15, ZSM-5, MgO was purchased from Shanghai Aladdin Biochemical Technology Co. Niobium pentoxide, methanol, dioxane were provided by Sinopharm Chemical Reagent Co. All of the above reagents were used directly without further treatment. The procedure for the preparation of the specimen of the product tetrahydrofuran-2,5-dicarboxylic acid dimethyl ester (THFDMC) is described in the supporting material (Scheme S1 and Fig. S1-2).

2. Preparation of Catalysts

In this work, the loaded Ru-based catalysts were prepared by the impregnation method. In a typical procedure for the preparation of Ru/HY: 0.1250 g of RuCl₃·3H₂O and 20 mL of deionized water were added to a 100 mL conical flask and stirred for 2-3 h. Subsequently, 1 g of support (HY, ZSM-5, Amberlyst-15, Nb₂O₅, MgO) was added and stirring was continued for 2 h. Then, 20 mL of aqueous sodium borohydride solution (1.7 wt%) was added dropwise to the mixture and stirred overnight. The loaded Ru-based catalyst (5 wt% theoretical loading) was filtered, washed, and dried overnight in a vacuum oven. Similarly, hexahydrate chloroplatinic acid or palladium chloride was also used as the catalyst precursors to prepare Pt or Pd-based catalyst by the same method described above.

In some cases, polyvinyl alcohol (PVA) was added as a dispersant to make the Ru loading more homogeneous (Scheme 1).

3. Catalyst Characterization

The relevant characterization methods for the catalysts are described in the supporting materials.

4. Catalyst Activity Test

The catalyst activity testing experiments in this work were carried out in a 25 mL stainless steel autoclave. The experimental procedure for the preparation of THFDMC by hydrogenation of FDMC was as follows: 0.5 mmol FDMC, 0.0920 g catalyst, and 7 mL methanol were mixed and sealed in an autoclave, and the reaction mixture was reacted under 3 MPa hydrogen pressure for 4 h, during which the system was heated and stabilized to 90 °C at 600 rpm. The reaction to cool to room temperature was allowed, and the solid catalyst in the reaction mixture was filtered, washed with ethanol three times and dried overnight in an oven at 110 °C to test the cyclic recovery performance of the catalyst.

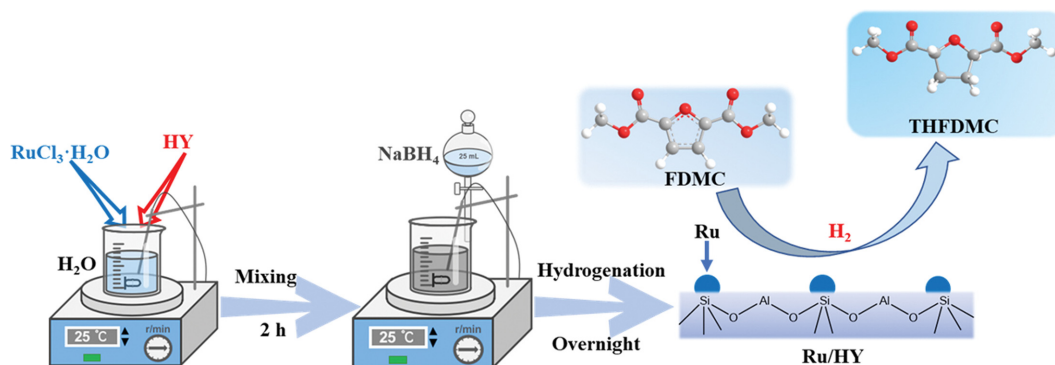
5. Product Analysis

The filtrate of the reacted mixture was analyzed qualitatively and quantitatively by dilution injection gas chromatography (GC) and gas chromatography-mass spectrometry (GC-MS). The GC model and test conditions were as follows: Agilent 7890, DB-WAXETR column (30 m × 250 μm × 0.25 μm), 1.0 mL/min N₂ as support gas. The heating procedure was as follows: the initial temperature was 40 °C, held for 4 min, and then increased to 250 °C at a heating rate of 10 °C/min, held for 2 min. The GC-MS model and test conditions were as follows: Thermofisher Trace 1300 gas chromatograph and ISQLT mass spectrometer, TR-5MS column (15 m × 250 μm × 0.25 μm), and 1.0 mL/min N₂ as support gas. The heating procedure was as follows: the initial temperature was 40 °C, held for 2 min, and then increased to 280 °C with a heating rate of 10 °C/min, held for 5 min. The quantification of FDMC, THFDMC is achieved by the calculation of an external standard curve corresponding to a certain concentration range of the standard. Correspondingly, yields and conversions are calculated by:

$$\text{FDMC conversion (\%)} = \left(1 - \frac{\text{mole of FDMC in the products}}{\text{initial mole of FDMC}}\right) \times 100$$

$$\text{THFDMC Yield (\%)} = \frac{\text{mole of THFDMC in the products}}{\text{initial mole of FDMC}} \times 100$$

$$\text{Carbon balance (\%)} = \frac{\sum \text{moles of C in products}}{\text{moles of C in FDMC converted}} \times 100$$



Scheme 1. Schematic illustration for the preparation procedure of the Ru/HY catalysts.

RESULTS AND DISCUSSION

1. Catalyst Characterization

In this research, three supports (HY, Amberlyst-15 and MgO) with different acidity and basicity were employed to load Ru. Figs. 1(a)-(c) show the XRD patterns of the prepared catalysts (Ru/HY, Ru/MgO, Ru/Amberlyst-15). The typical peaks at $2\theta=6.3^\circ$, 10.3° , 12.1° , 15.8° , 18.9° , 20.6° , 23.9° , 27.4° , 31.1° and 31.8° in Fig. 1(a) indicated that the zeolite structure of zeolite HY (PDF#88-2288) well remained after loading Ru [26], and the intensity of the diffraction peaks did not change significantly between HY and Ru/HY. No obvious diffraction peaks of Ru were observed in the XRD pattern of Ru/HY, which indicated that Ru species were well dispersed over the surface of HY. As illustrated in Fig. 1(b), the peaks at around 36.9° , 42.9° , 62.2° , 74.6° , 78.5° could be ascribed to MgO (PDF#74-1225), while the typical peaks about 18.6° , 32.8° , 38.0° , 50.8° , 58.6° , 62.0° , 68.2° , 72.0° , 81.2° were consistent with Mg(OH)₂ (PDF#83-0114). No diffraction peaks of Ru were observed in Fig. 1(b), indicating the fine dispersion of Ru over MgO. In contrast, the typical peaks at $2\theta=38.3^\circ$ and 44.0° in Fig. 1(c) were attributed to Ru (PDF#06-0663), suggesting that the agglomeration of Ru nanoparticles occurred to some extent over Amberlyst-15 as compared to that over HY or MgO.

The N₂ adsorption-desorption isotherms showed that all the supported Ru-based catalysts exhibited type IV isotherms and H₃ hysteresis loops, and had the pore sizes in the range of 2-50 nm, indicating the presence of mesoporous structures in these catalysts (Fig. S3 and Table 1). Ru/HY had a large specific surface area of 420.6 m²/g, in contrast, Ru/MgO or Ru/Amberlyst-15 gave a specific surface area of 40.97 m²/g or 36.08 m²/g, respectively. The surface areas of Ru-catalysts and supports (HY, MgO, Amberlyst-15) were close to the same, with 40.97 m²/g for Ru/MgO and 38.2 m²/g for its support. In addition, the pore volume for all the catalysts was similar, above 0.22 cm³/g, and the pore size of Ru/MgO was 22.17 nm.

The morphology of Ru/HY was observed by SEM. As shown in Fig. S4, irregular block structure in HY parent was clearly maintained after the loading of Ru. Notably, rough surface with numerous attachments was observed over the surface of Ru/HY (Fig. S4(a)-(b)), which can be ascribed to the formation of Ru nanoparticles over HY. In comparison, the addition of PVA as the dispersing agent brought about flat and smooth surface for Ru/HY catalyst (Fig. S4(c)-(d)), indicating the homogeneous dispersion of Ru species with the assistance of PVA.

The morphology and composition of Ru/HY, Ru/MgO, and Ru/Amberlyst-15 were further analyzed by HR-TEM and elemental mapping (EDS). As shown in Fig. 2(a), Ru nanoparticles with an average diameter of 2.13 nm were observed, and the lattice fringe

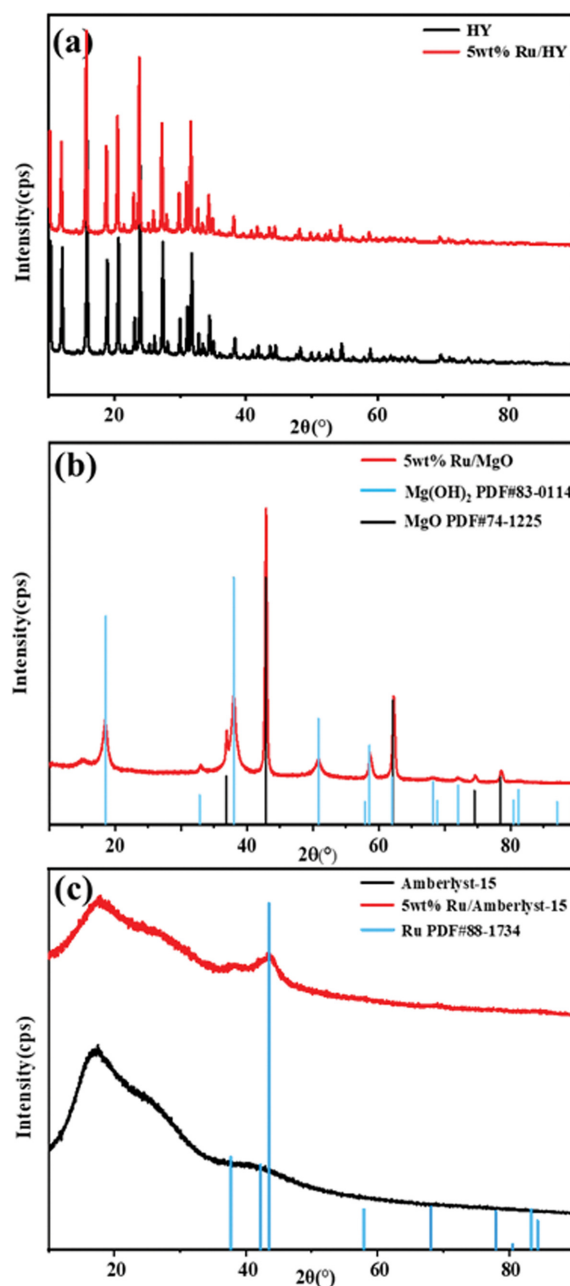


Fig. 1. X-ray diffraction (XRD) spectra of (a) 5 wt% Ru/HY, (b) 5 wt% Ru/MgO and (c) 5 wt% Ru/Amberlyst-15.

distance of the (101) lattice facet assigned to Ru nanoparticles of Ru/HY was determined to be 0.207 nm. Based on the STEM-EDS analysis (Fig. 2(d)-2(i)), a uniform dispersion of O, Si and Al was

Table 1. Textural properties of all tested catalysts

Samples	Ru content ^a (wt%)	S _{BET} ^b (m ² /g)	Support S _{BET} ^b (m ² /g)	Pore volume ^b (cm ³ /g)	Pore size ^b (nm)
5 wt% Ru/HY	4.18	420.6	405.3	0.260	2.47
5 wt% Ru/MgO	4.21	40.97	38.2	0.227	22.17
5 wt% Ru/Amberlyst-15	4.20	36.08	35.0	0.227	2.52

^aDetermined by ICP-AES. ^bDetermined by BET.

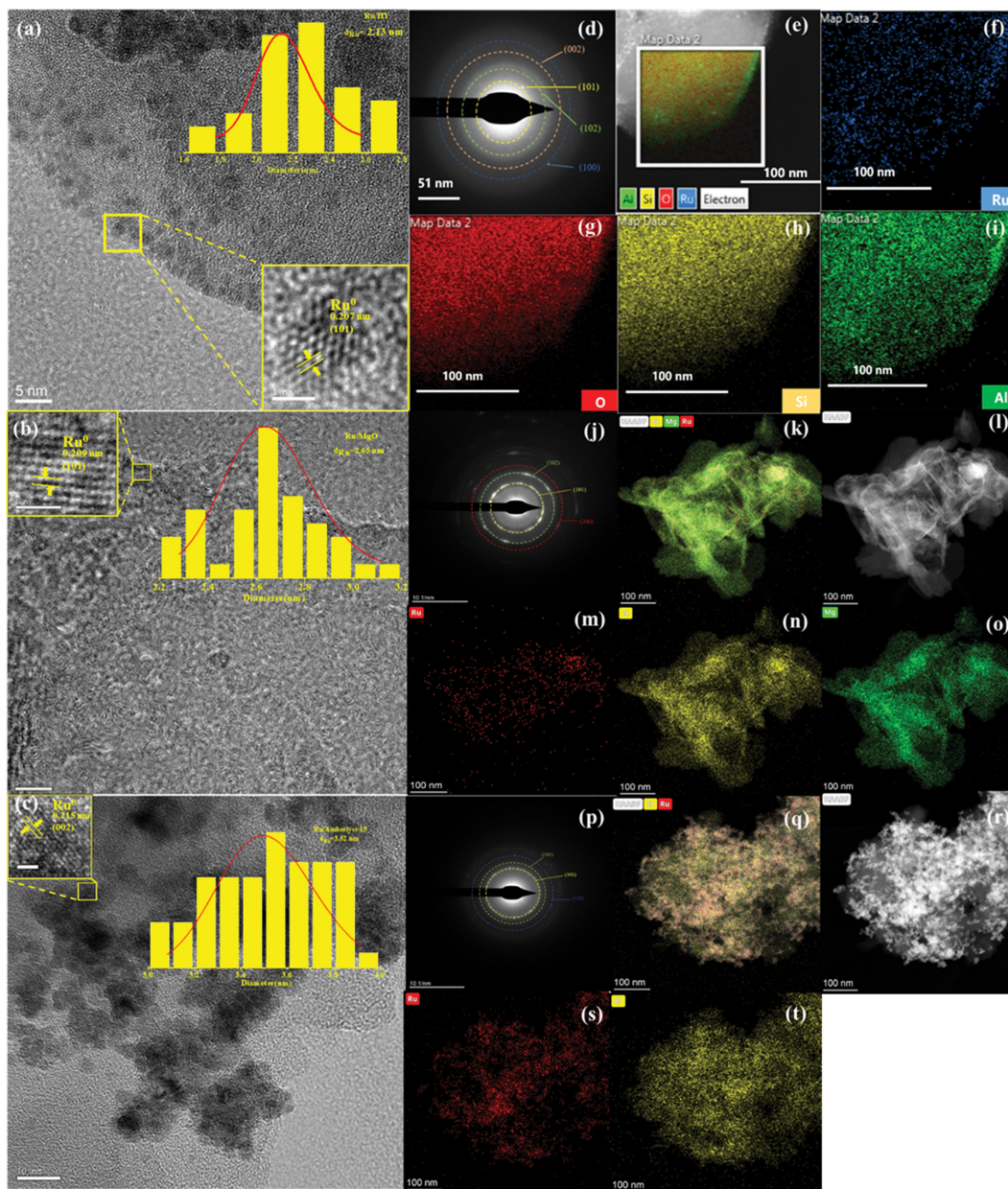


Fig. 2. (a) TEM images and elemental mapping images of 5 wt% Ru/HY (d)-(i); (b) 5 wt% Ru/MgO (j)-(o) and (c) 5 wt% Ru/Amberlyst-15 (p)-(t).

observed, while a slight agglomeration of Ru was found, which was highly consistent with the SEM images. In addition, Ru nanoparticles with lattice spacing of 0.209 nm (Fig. 2(b)) and 0.215 nm were attributed to the (101) crystal plane of Ru/MgO and the (002) crystal plane of Ru/Amberlyst-15. The highly dispersed Mg and O species over the catalysts could be observed from the elemental analysis (Fig. 2(k), (n), (o), (q), (t)), while Ru was agglomerated to different degrees in Ru/MgO (Fig. 2(m)) and Ru/Amberlyst-15 (Fig. 2(s)), especially Ru in Ru/Amberlyst-15 had a maximum average particle size of 3.52 nm and a larger agglomeration range, which was consistent with the results in XRD.

To investigate the acidic sites over the catalysts, NH_3 -TPD tests were performed in this study. It was known that the peaks below

250 °C and above 450 °C in the profile of NH_3 -TPD were associated to the weak and strong acidic sites, respectively. The NH_3 desorption peak in the region of 250–450 °C indicated the presence of moderately acidic sites. As shown in Fig. 3(a), two NH_3 desorption peaks are centered at 139 °C and 212 °C in the NH_3 -TPD profile of Ru/HY, which may be due to the reversible H-bonding adsorption process on the Brønsted acidic sites [27]. As shown in Fig. 3(a), the NH_3 desorption peak around 330 °C for Ru/MgO sample can be attributed to the NH_3 desorption from mesopore structure of MgO rather than acidity. The basicity of MgO supported catalyst can be evidenced by CO_2 -TPD. As shown in Fig. 3(c), the CO_2 desorption peak centered at 342 °C can be observed over Ru/MgO sample, which suggests the formation of a moderate basic site over Ru/

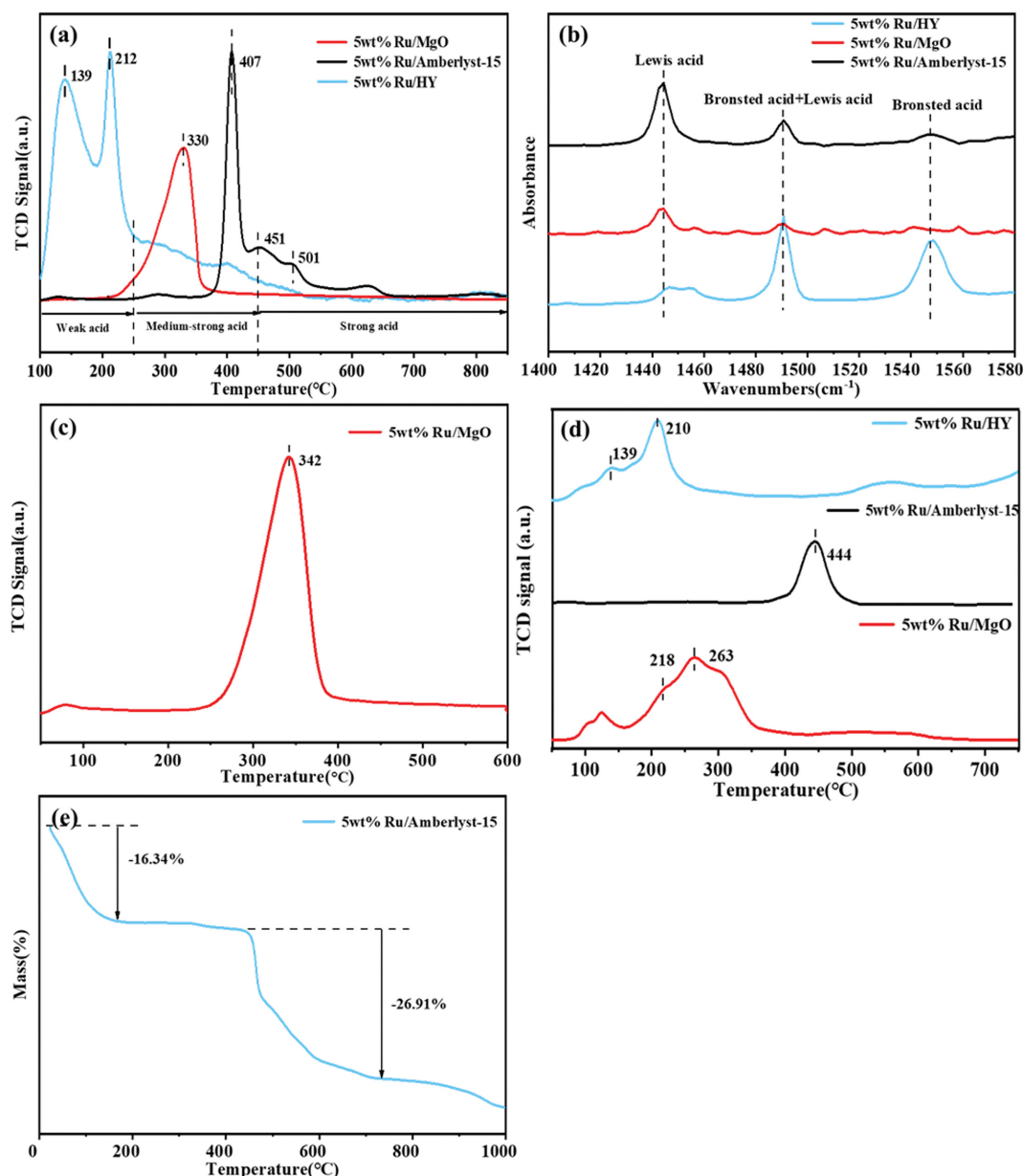


Fig. 3. (a) NH_3 -TPD, (b) Pyridine-adsorbed FTIR of 5 wt% Ru/HY, 5 wt% Ru/MgO, 5 wt% Ru/Amberlyst-15, (c) CO_2 -TPD of 5 wt% Ru/MgO, (d) H_2 -TPR of 5 wt% Ru/HY, 5 wt% Ru/MgO, 5 wt% Ru/Amberlyst-15, (e) TG of 5 wt% Ru/Amberlyst-15.

MgO [27]. Notably, several NH_3 desorption peaks above 400°C are observed in the NH_3 -TPD profile of Ru/Amberlyst-15, which should be probably attributed to the gaseous products formed by the degradation of Amberlyst-15 at elevated temperatures. On the other hand, it cannot be ruled out that there are strong acidic sites over Ru/Amberlyst-15. To further investigate the type of the acidic sites over these catalysts, the FTIR spectra of chemisorbed pyridine (Py-FTIR) were conducted in this work. As shown in Fig. 3(b), Ru/HY has an abundance of Brønsted acids with a hint of Lewis acids, and the Brønsted acids over Ru/HY should be ascribed to weakly acidic sites according to the NH_3 -TPD profile of Ru/HY (Fig. 3(a)), which probably originate from the HY support [28]. It is known that Amberlyst-15 can offer a wealth of Brønsted acidic sites. How-

ever, there are obvious Lewis acids with small amount of Brønsted acids over Ru/Amberlyst-15 (Fig. 3(b)), implying that original Brønsted acids over Amberlyst-15 were probably consumed during the loading of Ru, and the newly formed Lewis may be attributed the RuO_2 species. In addition, Lewis acids over Ru/Amberlyst-15 perhaps could be attributed to strong acidic sites according to the NH_3 -TPD profile of Ru/Amberlyst-15 (Fig. 3(a)).

The reducibility of Ru-based catalysts was further investigated by H_2 -TPR, and the presence of distinct H_2 consumption peaks suggests that the Ru species were not completely reduced by sodium borohydride during the catalyst preparation. As shown in Fig. 3(d), there are two H_2 consumption peaks centered at 218°C and 263°C in the H_2 -TPR profile of Ru/MgO, which can be allocated to the

consecutive reduction of $\text{RuO}_2\text{-RuO}_x\text{-Ru}^0$ [29]. These two peaks shift to lower temperature range (139°C and 210°C) in the case of Ru/HY, which could be mainly attributed to the medium interaction between HY and Ru species over Ru/HY as compared to that over Ru/MgO. Namely, there is stronger interaction between Ru species and HY over Ru/HY than that over Ru/MgO. In comparison, H_2 desorption peak below 300°C is missing in the case of Ru/Amberlyst-15, probably due to the completed reduction of Ru species over Ru/Amberlyst-15. In addition, a single peak around 444°C in the H_2 -TPR profile of Ru/Amberlyst-15 can be attributed to the degradation of Amberlyst-15 at elevated temperature (Fig. 3(e)).

The chemical states of the surface elements over the catalysts were further studied by XPS. As shown in Fig. 4, the peaks at 462.78,

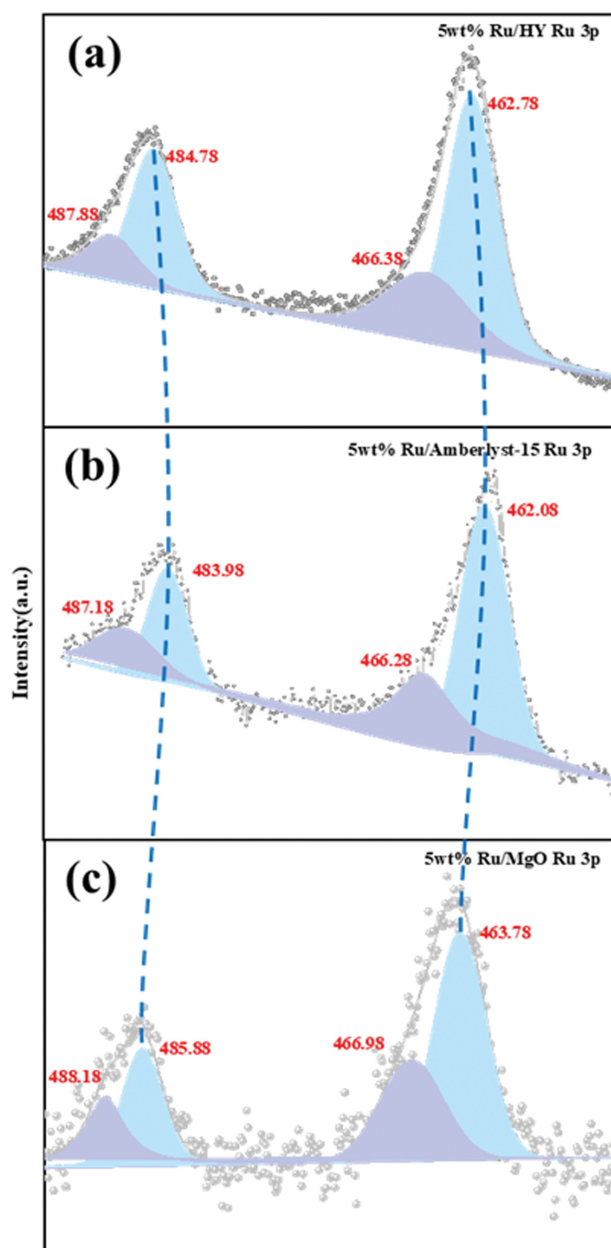


Fig. 4. XPS spectra of Ru 3p in (a) 5 wt% Ru/HY, (b) 5 wt% Ru/Amberlyst-15, (c) 5 wt% Ru/MgO.

484.78, 466.38, and 487.88 eV in the XPS spectrum of Ru/HY are attributed to $\text{Ru}^0 3p_{3/2}$, $\text{Ru}^0 3p_{1/2}$, $\text{Ru}^{4+} 3p_{3/2}$ and $\text{Ru}^{4+} 3p_{1/2}$, respectively [30]. These peaks move to lower binding energy range in the case of Ru/Amberlyst-15; however, these peaks shift to higher binding energy range for Ru/MgO. The above finding indicates the presence of medium interaction between Ru species and HY over Ru/HY among these three catalysts. Further analysis showed that the surface $\text{Ru}^{4+}/\text{Ru}^0$ ratio of Ru/HY was 0.36, which was much smaller than those for Ru/Amberlyst-15 (0.56) and Ru/MgO (0.53). Therefore, there are more metallic Ru species over Ru/HY, which is more favorable for the hydrogenation reaction.

2. Catalyst Screening

It is known that the nature of the supports has significant influence on the catalytic performance of the supported catalysts. In the present work, noble metals supported on the supports with different acidity and basicity were prepared and employed for the hydrogenation of FDMC. The route of synthesizing THFDMC from FDMC is shown in Fig. 5(a).

As shown in Fig. 5, Ru/HY outperformed Pd/HY and Pt/HY, and gave a desirable THFDMC yield of 99.4% at a completed FDMC conversion (90°C , 3 MPa H_2 , 4 h). Besides HY, Amberlyst-15, ZSM-5, MgO, Nb_2O_5 were also applied as the support for Ru, and their catalytic activity was evaluated for the hydrogenation of FDMC under the identical conditions. As shown in Fig. 5, Ru supported on neutral activated carbon (Ru/C) offered the minimum FDMC conversion (24.6%) and THFDMC yield (21.9%). Ru supported on basic MgO (Ru/MgO) gave a moderate FDMC conversion of 73.9% with a THFDMC yield of 73.9%. Apparently, Ru supported on acidic supports, such as HY, ZSM-5 and Amberlyst-15, provided better catalytic performance among these Ru-based catalysts. For instance, a

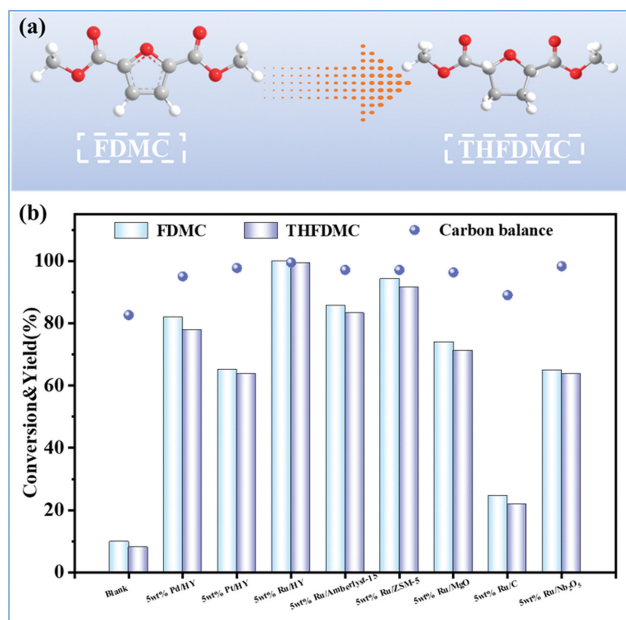


Fig. 5. (a) Schematic illustration of the pathways for the THFDMC production from FDMC, (b) Catalytic conversion of FDMC to THFDMC over different catalysts. Reaction conditions: 0.5 mmol FDMC, 0.0920 g catalyst, 7 mL methanol, 90°C , 3 MPa H_2 , 4 h.

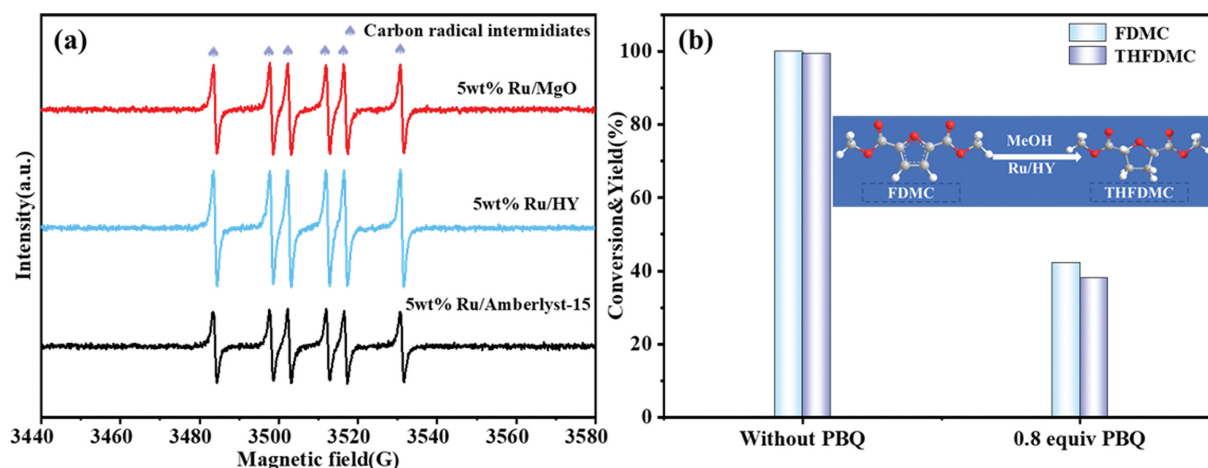


Fig. 6. (a) EPR spectra of a radical capture experiment in which only FDMC was activated on catalysts. (b) The hydrogenation of FDMC to THFDMC with or without PBQ. Conditions: FDMC (0.5 mmol), 5 wt% Ru/HY (5.5 mol% metal relative to FDMC), methanol 7 mL, 90 °C, H₂ 3 MPa, 4 h.

FDMC conversion was 85.7% with a THFDMC yield of 83.2% was also obtained over Ru/Amberlyst-15.

The acid-base property of the supports plays an important role on the catalytic performance of the noble metals supported catalysts for hydrogenation reactions. In this context, Ru catalysts supported on representative supports such as HY, Amberlyst-15 and MgO were systematically characterized. Notably, Ru/HY showed weak Brønsted acid sites with the largest specific surface area (Table 1, Fig. 3); combining the analysis results of XPS (Fig. 4), Ru/HY has weak Brønsted acid sites with the largest specific surface area (Table 1, Fig. 3), leading to the formation of surface electron deficiency. Notably, Ru³⁺ reduced could generate abundant low-coordinated Ru sites, and then thus promote the redispersion of Ru, thereby facilitating the enhanced dispersion of Ru species on HY [27]. More importantly, Ru/HY offered a surface Ru⁴⁺/Ru⁰ ratio much lower than other catalysts (Fig. 4(a)), which could largely favor the activation of hydrogen and then promote the hydrogenation of FDMC over Ru/HY.

The hydrogenation of furan ring could take place through radical intermediates. In this light, DMPO was used as a trapping agent and electron paramagnetic resonance (EPR) analysis was conducted. As shown in Fig. 6(a), only carbon radical intermediates signals were detected in the EPR tests, and the strongest signal intensity can be observed in the EPR spectrum of Ru/HY, followed by Ru/MgO and Ru/Amberlyst-15.

To further reveal the effect of carbon radical intermediates on the hydrogenation of FDMC, radical capture experiments were performed in the reaction system. As shown in Fig. 6(b), the addition of free radical scavenger p-benzoquinone PBQ before the reaction resulted in a dramatic drop of FDMC conversion (42.3%) and THFDMC yield (38.0%). The above finding suggests that the promotion effect of Ru/HY on the formation of carbon radical intermediates should also be partially responsible for its outstanding performance for the hydrogenation of FDMC.

In view of the excellent catalytic performance of Ru/HY in Fig. 5, it was determined that the active metal element was selected as

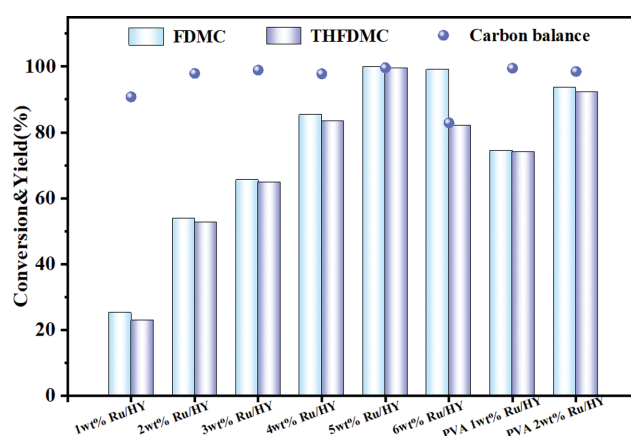


Fig. 7. Catalytic conversion of FDMC to THFDMC over different Ru loading catalysts. Reaction conditions: 0.5 mmol FDMC, 0.0920 g catalyst, 7 mL methanol, 90 °C, 3 MPa H₂, 4 h.

Ru and the support was zeolite HY. Subsequently, the effect of THFDMC yield with Ru loading was explored (Fig. 7). The yield of THFDMC gradually increased with the increase of Ru loading (theoretical value) from 22.9% (1 wt% Ru/HY) to 99.4% (5 wt% Ru/HY), which gradually decreased to 82.2% with the increasing Ru loading to 6 wt%, probably because of the agglomeration of Ru. It is worth mentioning that with the addition of the dispersant polyvinyl alcohol (PVA), the yield of THFDMC obtained over PVA 2 wt% Ru/HY (92.3%) increased by 39.5% compared to that achieved over 2 wt% Ru/HY when the Ru loading was 2 wt%.

3. Effect of Reaction Parameters on Hydrogenation

High yields (99.4%) of THFDMC can be obtained from FDMC at 90 °C under 3 MPa H₂. As shown in Fig. 8(a), the yield of THFDMC clearly shows an increasing trend with the increase of hydrogen pressure at low temperature of 90 °C. For example, the yield of THFDMC increased from none (no H₂) to 99.4% with the H₂ pressure increasing to 3 MPa H₂. The effect of reaction temperature ranging from 80–130 °C was also examined for the selective conversion

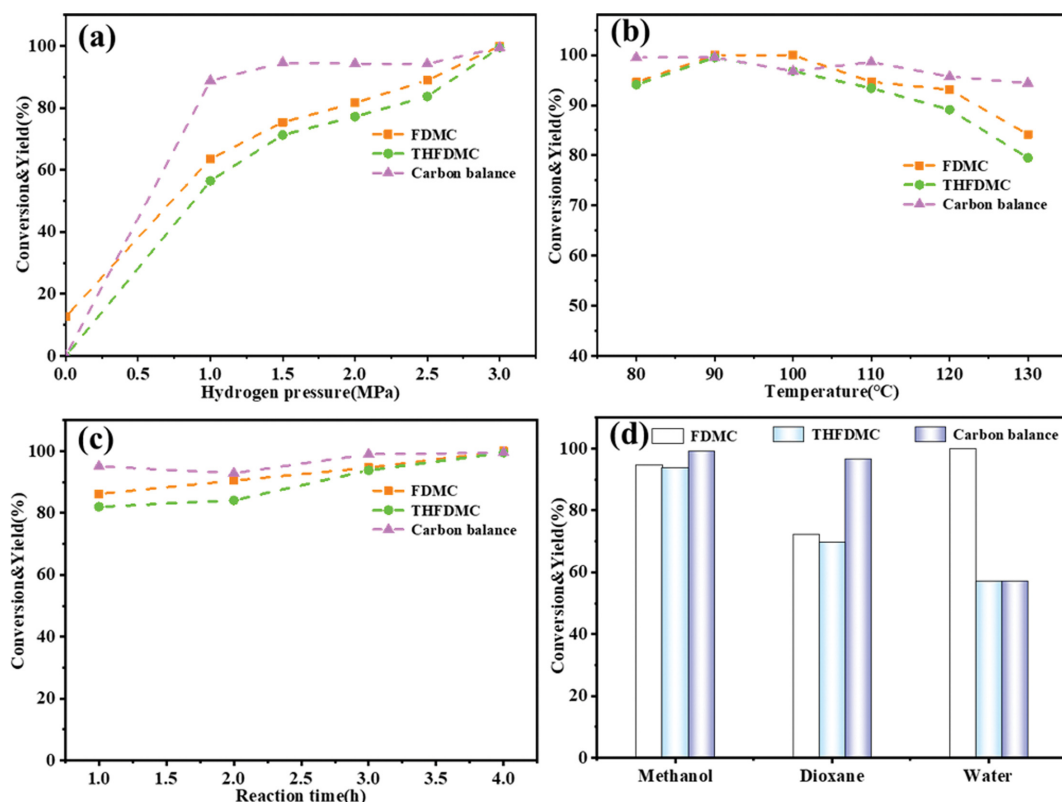


Fig. 8. Optimization of reaction conditions for the FDMC hydrogenation with 5 wt% Ru/HY. (a) Hydrogen pressure; (b) Reaction temperature; (c) Reaction time; (d) Solvent screening experiments. The reaction conditions for (a): FDMC (0.5 mmol), 5 wt% Ru/HY (0.0920 g), 90 °C, 4 h, methanol 7 mL; The reaction conditions for (b): FDMC (0.5 mmol), 5 wt% Ru/HY (0.0920 g), 3 MPa H₂, 4 h, methanol 7 mL; The reaction conditions for (c): FDMC (0.5 mmol), 5 wt% Ru/HY (0.0920 g), 3 MPa H₂, 90 °C, methanol 7 mL. The reaction conditions for (d): FDMC (0.5 mmol), 5 wt% Ru/HY (0.0920 g), 3 MPa H₂, 90 °C, 3 h, solvents 7 mL.

of FDMC to THFDMC. Increasing the temperature can increase the yield of THFDMC in a certain range (Fig. 8(b)); when the temperature was increased from 80 °C to 90 °C, the yield of THFDMC increased from 94.1% to 99.4%, while the conversion of FDMC decreased from 100% to 84.2% when the temperature continued to increase after 90 °C, especially when the temperature increased to 130 °C, and the yield of THFDMC also decreased from 99.4% to 79.5%. This indicated that high temperature was not suitable for the preparation of THFDMC, which may be due to the reduction of catalyst activity caused by coking on the catalyst surface during the reaction [31]. While extending the reaction time could improve the conversion of FDMC (Fig. 8(c)), the yield of THFDMC in methanol reached a maximum of 99.4% after 4 h of reaction at 90 °C (Fig. 8(d)).

4. Reusability Tests of Catalyst

After the reaction, the catalyst was separated out by centrifugation, followed by washing thoroughly with ethanol, and then drying in oven (110 °C, 12 h) for the next run test. The yield of THFDMC only decreased by 9.1% (from 99.4% to 90.3%) over the 5th recycled catalyst comparable to that achieved over the fresh catalyst (Fig. 9), These findings indicated that Ru/HY catalyst was stable during the production of THFDMC from FDMC.

5. Substrate Scope of Ru Catalyst

Because of the exceptional catalytic activity of Ru/HY, we next

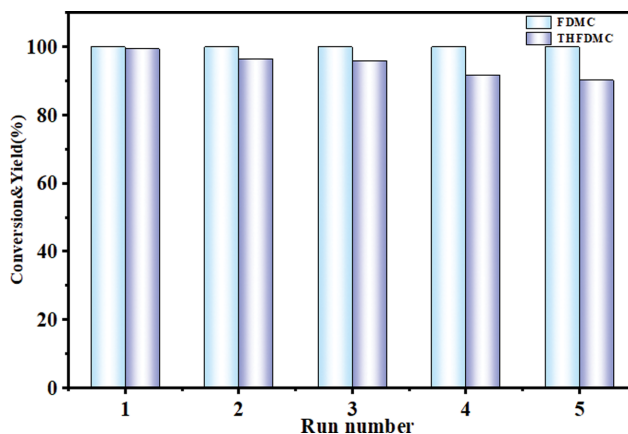
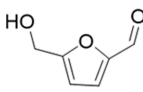
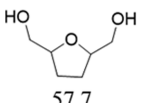
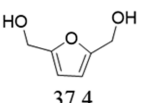
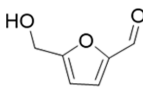
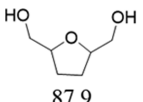
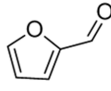
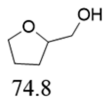
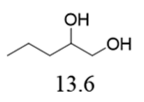
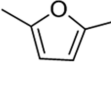
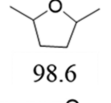
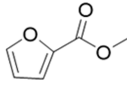
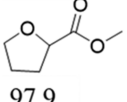
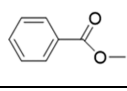
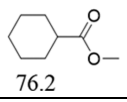
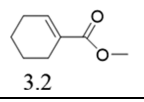


Fig. 9. The cyclic recovery experiments of catalyst Ru/HY. Reaction conditions were as follows: FDMC (0.5 mmol), 5 wt% Ru/HY (0.0920 g), 3 MPa H₂, 90 °C, 4 h, methanol 7 mL.

explored the feasibility of using this catalyst in other situations by evaluating the range of substrates (including 5-hydroxymethylfurfural, furfural, 2,5-dimethylfuran, 2-furoate, and methyl benzoate) and the tolerance of the four functional groups (Table 2 and Figs. S5-8). Overall, this range proved to be more versatile, and the hydrogenation of these furan-like cyclic compounds and benzene cyclic

Table 2. Hydrogenation of various substrates catalyzed by 5 wt% Ru/HY^a

Entry	Substrate	Conv. (%)	Product (%)	Carbon balance (%)	
1		>99.9	 57.7	 37.4	95.2
2 ^b		95.3	 87.9		92.2
3		>99.9	 74.8	 13.6	88.4
4		>99.9	 98.6		98.6
5		>99.9	 97.9		97.9
6		80.5	 76.2	 3.2	98.6

^aThe reaction conditions: substrates 0.5–1 mmol, 5 wt% Ru/HY 0.0920 g, 3 MPa H₂, 4 h, 90 °C, methanol 7 mL; ^bHMF 1 mmol, Ru/HY 0.0920 g, 3 MPa H₂, 4 h, 90 °C, Water 7 mL.

compounds yielded the desired products with better efficiency and higher carbon balance. Overall, the yield of fully hydrogenated products of cyclic compounds is still relatively high, allowing to verify a wide range of substrates and solvents as well as excellent functional group tolerance [32].

CONCLUSION

Ru-based catalysts loaded on HY, MgO and Amberlyst-15 were prepared by impregnation for the complete hydrogenation of FDMC, and the effect of support properties on the electron density and state of Ru and catalyst performance was investigated. The optimal reaction conditions were determined to be 90 °C and 3 MPa hydrogen pressure for 4 h, the best yield of THFDMC was obtained as 99.5%. Various characterizations indicate that the weak Brønsted acidic support HY interacts with the metal Ru to promote the electron density reduction and the Ru⁴⁺/Ru⁰ ratio of Ru/HY is minimized, which facilitates the hydrogenation reaction. In addition, the hydrogenation process generates carbon radical intermediates, and Ru/HY has the highest intensity of carbon-centered peaks, which further explains its best effect. The catalyst was also found to be suitable for the hydrogenation of other cyclic compounds, capable of verifying a wide range of substrates and solvents and excellent functional group tolerance, with excellent recycling performance of the catalyst.

ACKNOWLEDGEMENTS

We are grateful for the funding supported by the National Natural

Science Foundation of China (Grant nos. U22A20421; 22078275), the Fundamental Research Funds for the Central Universities (Grant no. 20720220065).

SUPPORTING INFORMATION

Additional information as noted in the text. This information is available via the Internet at <http://www.springer.com/chemistry/journal/11814>.

REFERENCES

1. F. Li, X.-L. Li, C. Li, J. Shi and Y. Fu, *Green Chem.*, **20**, 3050 (2018).
2. X. Yu, H. Liu, Q. Wang, W. Jia, H. Wang, W. Li, J. Zheng, Y. Sun, X. Tang, X. Zeng, F. Xu and L. Lin, *ACS Sustain. Chem. Eng.*, **9**, 13176 (2021).
3. Y. Queneau and B. Han, *Innovation (Camb)*, **3**, 100184 (2022).
4. S. Li, M. Dong, M. Peng, Q. Mei, Y. Wang, J. Yang, Y. Yang, B. Chen, S. Liu, D. Xiao, H. Liu, D. Ma and B. Han, *Innovation (Camb)*, **3**, 100189 (2022).
5. S. Kim, Y.F. Tsang, E. E. Kwon, K.-Y. A. Lin and J. Lee, *Korean J. Chem. Eng.*, **36**, 1 (2018).
6. S. Sadjadi, V. Farzaneh, S. Shirvani and M. Ghashghaee, *Korean J. Chem. Eng.*, **34**, 692 (2017).
7. X. Lv, J. Xiao, T. Sun, X. Huo, M. Song and L. Shen, *Korean J. Chem. Eng.*, **35**, 394 (2017).
8. W. Yu, Y.-P. Hsu and C.-S. Tan, *Appl. Catal., B*, **196**, 185 (2016).
9. A. Salazar, P. Hunemorder, J. Rabeah, A. Quade, R. V. Jagadeesh and E. Mejia, *ACS Sustain. Chem. Eng.*, **7**, 12061 (2019).

10. T. Dimitriadis, D. N. Bikiaris, G. Z. Papageorgiou and G. Floudas, *Macromol. Chem. Phys.*, **217**, 2056 (2016).
11. S. K. Burgess, J. E. Leisen, B. E. Kraftschik, C. R. Mubarak, R. M. Krieger and W. J. Koros, *Macromolecules*, **47**, 1383 (2014).
12. A. Codou, M. Moncel, J. G. van Berkel, N. Guigo and N. Sbirrazzuoli, *Phys. Chem. Chem. Phys.*, **18**, 16647 (2016).
13. C. F. Araujo, M. M. Nolasco, P. J. A. Ribeiro-Claro, S. Rudić, A. J. D. Silvestre, P. D. Vaz and A. F. Sousa, *Macromolecules*, **51**, 3515 (2018).
14. G. Z. Papageorgiou, D. G. Papageorgiou, Z. Terzopoulou and D. N. Bikiaris, *Eur. Polym. J.*, **83**, 202 (2016).
15. H. Liu, X. Tang, X. Zeng, Y. Sun, X. Ke, T. Li, J. Zhang and L. Lin, *Green Energy Environ.*, **7**, 900 (2022).
16. S. S. R. Gupta, A. Vinu and M. L. Kantam, *J. Catal.*, **389**, 259 (2020).
17. D. Zhao, T. Su, C. Len, R. Luque and Z. Yang, *Green Chem.*, **24**, 6782 (2022).
18. W. Xie, B. Chen, W. Jia, H. Liu, Z. Li, S. Yang, X. Tang, X. Zeng, Y. Sun, X. Ke, T. Li, H. Fang and L. Lin, *J. Energy Chem.*, **75**, 95 (2022).
19. Y. Nakagawa, M. Yabushita and K. Tomishige, *Trans. Tianjin Univ.*, **27**, 165 (2021).
20. Q. Yuan, K. Hiemstra, T. G. Meinds, I. Chaabane, Z. Tang, L. Rohrbach, W. Vrijburg, T. Verhoeven, E. J. M. Hensen, S. van der Veer, P. P. Pescarmona, H. J. Heeres and P. J. Deuss, *ACS Sustain. Chem. Eng.*, **7**, 4647 (2019).
21. C. Chien Truong, D. Kumar Mishra, S. Hyeok Ko, Y. Jin Kim and Y. W. Suh, *ChemSusChem*, **15**, e202200178 (2022).
22. H. Kataoka, D. Kosuge, K. Ogura, J. Ohyama and A. Satsuma, *Catal Today*, **352**, 60 (2020).
23. G. Bottari, A. J. Kumalaputri, K. K. Krawczyk, B. L. Feringa, H. J. Heeres and K. Barta, *ChemSusChem*, **8**, 1323 (2015).
24. D. K. Mishra, H. J. Lee, C. C. Truong, J. Kim, Y. W. Suh, J. Baek and Y. J. Kim, *Mol. Catal.*, **484**, 110722 (2020).
25. N. Perret, A. Grigoropoulos, M. Zanella, T. D. Manning, J. B. Claridge and M. J. Rosseinsky, *ChemSusChem*, **9**, 521 (2016).
26. A. Wang, P. Berton, H. Zhao, S. L. Bryant, M. G. Kibria and J. Hu, *ACS Sustain. Chem. Eng.*, **9**, 16115 (2021).
27. Y. He, J. Fan, J. Feng, C. Luo, P. Yang and D. Li, *J. Catal.*, **331**, 118 (2015).
28. L. Wang, L. Lian, H. Yan, F. Wang, J. Wang, C. Yang and L. Ma, *RSC Adv.*, **9**, 30335 (2019).
29. S. Jin, Z. Xiao, C. Li, C. T. Williams and C. Liang, *J. Energy Chem.*, **23**, 185 (2014).
30. J. Zhang, X. Mao, S. Wang, L. Liang, M. Cao, L. Wang, G. Li, Y. Xu and X. Huang, *Angew. Chem. Int. Ed.*, **61**, e202116867 (2022).
31. S. Fulignati, C. Antonetti, E. Wilbers, D. Licursi, H. J. Heeres and A. M. Raspolli Galletti, *J. Ind. Eng. Chem.*, **100**, 390.e1 (2021).
32. X. L. Dong, Y. F. Jia, M. Y. Zhang, S. Q. Ji, L. P. Leng, J. H. Horton, C. Xu, C. He, Q. Tan, J. W. Zhang and Z. J. Li, *Chem. Eng. J.*, **451**, 138660 (2023).